

Radially Periodic Metasurface Lenses for Magnetic Field Collimation in Resonant Wireless Power Transfer Applications

I. V. Soares¹, U. C. Resende²

¹*Institut d'Electronique et des Technologies du Numérique, University of Rennes 1, France
icaro.soares@ieee.org*

²*Department of Electrical Engineering, Federal Center for Technological Education of Minas Gerais, Brazil
resendeursula@cefetmg.br*

Abstract— In this paper, a new procedure and topology of magnetic metasurface lens are proposed for improving the performance of Resonant Wireless Power Transfer systems. Firstly, three subwavelength unit cells are optimized in order to get negative magnetic permeability in the same frequency, each one with a different refractive index, and they are experimentally characterized. Then, the Transformation Optics technique is applied in order to find the unit cell arrangements which lead to the magnetic field focusing in a given direction. For this purpose, two coordinate transformations are proposed, and the effective electric permittivity and permeability that generate these profiles are calculated. It is shown from simulations and measurements that the refractive index gradient produced by the radial disposition of the unit cells can lead to a magnetic field manipulation similar to the optical converging and diverging lenses. Both metamaterials lenses are built, and the calculation of the magnetic flux density as a function of the measured induced voltage in a probe coil verifies their effects on the magnetic field. Finally, their performance in a resonant wireless power transfer system is tested, and improvements in terms of efficiency and range are presented. The proposed design method and the lenses that were developed demonstrate that metasurface lenses can improve efficiency without reducing the range, once these lenses are positioned close to the transmitter coil. Besides that, this method can reduce the losses due to misalignment between coils once the field can be collimated in a specific direction.

Index Terms— Lens, metamaterials, subwavelength unit cells, transformation optics, wireless power transfer.

I. INTRODUCTION

Resonant Wireless Power Transfer (RWPT) is a technology for transmitting and receiving electrical energy through resonant coupled coils in the near-field region. The first attempts to the physical realization of these systems were carried out by Nicola Tesla, who also filed the first patent [1]. Since 1960, it has been used for medical implants, induction heaters, radio-frequency identification tags, and charging of portable electronic devices, among other applications [2]. For many commercial applications, the transmission coil is close to the receiver because the efficiency is higher in these cases. However, as this efficiency decreases proportionally with the inverse cube of distance [3], RWPT still is restricted to short and mid-range systems in which the distance between coils is less or equal to the coil size. In order to overcome this limitation, different enhancement techniques have been developed.

One way to improve RWPT systems is by using metamaterials. Although a closed definition has not been agreed yet, it can be stated that metamaterial is a composite material, with a periodic or non-periodic structure whose unconventional electromagnetic behavior is due to its unit cell disposition and chemical composition [4]. Such medium was conceived by Victor Veselago [5] that investigated the electrodynamic behavior of left-handed media, i.e. a medium with negative magnetic permeability (μ) and electric permittivity (ϵ). However, it was only after the realization of negative permittivity by using a wire medium [6], and negative permeability with Split Ring Resonators (SRR) [7] that this concept caught up the attention of the scientific community.

Nowadays, metamaterials have been used in invisibility cloak [8], frequency selective surfaces [9], leaky-wave antennas [10], and superlenses [11], among other applications. The idea of a lens that can overcome the optical limitation, i.e. the smaller area that it focuses light is λ^2 (λ = wavelength) was proposed in [12]. These superlens made of left-handed media was firstly applied to enhance RWPT systems in [13]. The metamaterial lens acts by reducing the evanescent field decay in the near-field region, thus improving energy transfer efficiency.

In this work, new metamaterial lenses with $\mu < 0$ are proposed for focusing magnetic field in RWPT applications. At first, three unit cells with different sizes but operating at the same frequency are designed and characterized. These different unit cells are used in order to produce a refractive index gradient. Then, transformation optics technique is applied to conceive the unit cell distribution that makes a flat lens operating as converging or diverging lens. Both lens prototypes are built, and the magnetic flux density calculated from induced voltage measurement is used to verify their behavior. Finally, these lenses are tested in an RWPT system, and improvements in power transfer efficiency are evaluated in terms of frequency and distance between transmitter and receiver coils.

Previous works have demonstrated that metamaterial lenses can improve RWPT efficiency and range [14]–[16]. However, the novelty of this paper is in the fact that it proposes a procedure to design metamaterial lenses which can collimate the magnetic field in a specific direction. It is particularly beneficial for wireless power transfer applications, once the possibility of focusing the magnetic field lines enables using transmitter and receiver coils with different sizes and alignments. Moreover, in most of the works, the metamaterial slab is positioned in the middle of the RWPT system [17]–[19], which may compromise the transmission range. Nonetheless, in the proposed application, the lenses are positioned in front of the transmitter coil.

II. UNIT CELL DESIGN AND CHARACTERIZATION

The first step to project a metasurface is to design a unit cell in which induced currents emulate atomic resonances. In order to achieve this operation, it is required that the unit cell size shall be less than a tenth of the free-space wavelength, λ_0 . Nevertheless, in this work, it is designed subwavelength unit cells (size $\ll \lambda_0$). It is pointed out in [12] that, for such cases, electric and magnetic field are decoupled; therefore the double negative condition for superlens can be relaxed and $\mu < 0$ is enough to produce an artificial magnetic medium.

One of the most commonly used structures for this purpose is the Split Ring Resonator (SRR). However, to operate at dozens of megahertz, this topology would be prohibitively large. Therefore, an inner spiral was included in the topology as well as a lumped capacitor in order to get a more compact structure [20]. Consequently, the resonant frequency can be adjusted by varying the number of turns

and the lumped capacitance, C . The proposed SRR-spiral topology is presented in Fig. 1(a). The inner spiral is described by Eq. 1, where t is a real angle parameter, and ϕ_1 and ϕ_2 are the initial and final angles of the spiral.

$$\begin{cases} x(t) = 0.2t \cos(t) \\ y(t) = 0.2t \sin(t) \\ z(t) = 0 \end{cases}, \phi_1 \leq t \leq \phi_2. \quad (1)$$

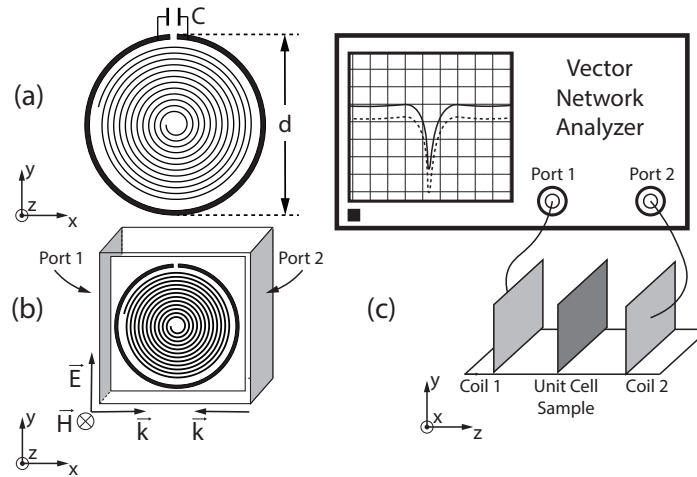


Fig. 1. Unit cell design and characterization: (a) SRR-spiral topology, (b) simulation setup and boundary conditions and (c) μ measurement setup.

Once the unit cell topology was proposed based on the physical properties of the SRR and the spiral, its dimensions must be optimized in order to match the design requirements. This optimization aims to obtain a negative value for the real magnetic permeability, i.e. $\Re(\mu) < 0$, taking into account the operating frequency $f \leq 20 \text{ MHz}$. In this case, the optimized parameters are the SRR diameter d , the initial ϕ_1 and final ϕ_2 spiral angles, and the lumped capacitance C . However, once the capacitor must be chosen within its commercial values when the optimization algorithm is close to the convergence, the capacitance is fixed in the closest commercial value, and the optimization algorithm is resumed only with the geometrical parameters. This optimization problem is summarized in Eq. 2.

$$\begin{aligned} & \underset{\hat{\mathbf{x}}}{\text{maximize}} && -\Re[\mu(\hat{\mathbf{x}})] \\ & \text{where} && \hat{\mathbf{x}} = [f, \phi_1, \phi_2, d, C] \\ & \text{subject to} && f \leq 20 \text{ MHz} \\ & && C \in \{\text{commercial values}\} \end{aligned} \quad (2)$$

For this optimization, the objective function is evaluated through the metamaterial homogenization function in the software Computer Simulation Technology (CST[®]) that returns μ and ε based on the simulated scattering parameters. The optimization method applied is the Covariance Matrix Adaptation Evolutionary Strategy that is also implemented in CST[®]. For this algorithm, the parameter $0 \leq \sigma \leq 0.9$ controls the step size, so that closer to zero, the optimization is more local, whereas closer to 0.9 forces the method to be more global. Therefore, in this optimization, the parameter σ was set to 0.9.

Due to the limited commercial values, the optimal parameters for the unit cell 1 (UC 1) were obtained for the operating frequency of 16.125 MHz. After that, two other larger unit cells (UC 2 and UC 3) were optimized, fixing the frequency to 16.125 MHz. Since the lumped capacitance is inversely proportional to the cell size, a new constraint was set to obtain larger unit cells: C must be lower than the one obtained for UC 1. The parameters obtained after the optimization of all three unit cells are summarized in Table I.

TABLE I. UNIT CELL (UC) CONSTRUCTIVE PARAMETERS: SPIRAL INITIAL (ϕ_1) AND FINAL (ϕ_2) ANGLES, LUMPED CAPACITANCE (C), SPLIT-RING DIAMETER (d), AND EFFECTIVE REFRACTIVE INDEX (n)

UC	ϕ_1	ϕ_2	C	d	n
1	690.998°	5000°	1 nF	$\lambda_o/478$	37.841
2	969.958°	6059.81°	820 pF	$\lambda_o/402$	46.532
3	1000°	8319.284°	560 pF	$\lambda_o/293$	61.236

In the simulation, it was considered that the unit cells were printed over a single-sided copper fiberglass substrate, FR4, with characterized relative electric permittivity $\epsilon_r = 4.3$ and loss tangent $\delta = 0.01$; the dielectric layer thickness is 1.6 mm and the conductive layer thickness is 20 μm . All simulations were carried out using the frequency domain solver of CST[®], which is based on the finite element method with adaptive tetrahedral mesh refinement. To simulate these structures, the unit cell was centered between two parallel waveguide ports; perfect electrically conducting boundary conditions were set on the faces that are perpendicular to the electric field (\vec{E}) and perfect magnetically conducting on the faces that are perpendicular to the magnetic field (\vec{H}) [21], as indicated in Fig. 1(b) where \vec{k} is the wave vector. These boundary conditions and the port positioning are most indicated to single-negative magnetic ($\mu < 0, \epsilon > 0$) unit cells once it reproduces the setup for experimental characterization and physical application of the metasurfaces built with them. Considering these settings, the magnetic field is perpendicular to the unit cell, and surface currents are induced in the SRR-Spiral metalization, thus producing a magnetic moment perpendicular to the loop. Once the unit cells are subwavelength, the interaction between the induced magnetic moments gives rise to the properties of the magnetic metasurfaces [22].

The three simulated unit cells were built through the etching process, using the dimensions presented in Table I and the FR4 substrate previously described. In order to characterize these unit cells and to verify the frequency in which $\mu < 0$, the method presented in [23] was applied. It consists of two printed coils, coaxially aligned, each one connected to a port of the Agilent E5071C Vector Network Analyzer (VNA), as indicated in Fig. 1(c). The set of measured S-parameters without the presence of unit cells is used as a reference. After that, a single unit cell sample is inserted between the coils, and the same measurement is performed. This procedure is then repeated for each one of the designed unit cells. From these measurements, the effective complex magnetic permeability, μ , can be extracted using Eq. 3:

$$\mu = \frac{\Re(S_{21_s}) + j\Im(S_{21_s})}{\Re(S_{21_r}) + j\Im(S_{21_r})}, \quad (3)$$

where $\Re(S_{21})$ and $\Im(S_{21})$ are the real and imaginary parts of the reverse complex transmission coefficient (S_{21}). In addition, the indices r and s indicate the reference measurement and the measurement with the unit cell sample, respectively.

The effective permeability calculated from S-parameters measurement for the three designed unit cells are shown in Fig. 2. As can be noticed, the negative permeability for all unit cells is between 15 and 16 MHz, as expected. The deviations between them result from constructive parameters uncertainties and the deviation on the capacitance value within its tolerance (10 – 20%). In order to choose the operating frequency for the system, this deviation must be taken into account and the fact that, when the real part of the effective permeability $\Re(\mu)$ becomes more negative, its imaginary part $\Im(\mu)$, which is associated with losses, becomes more positive. Therefore, a trade-off between these two components must be found. The most common approach in the literature is to use the frequency in which $\mu = -1$ [12], [24]. However, setting this as an objective function in the optimization step is not feasible due to the unpredictability of deviations found in the experimental realization. In this way, the operation frequency is chosen to be 15.53 MHz since at this frequency, all unit cells present negative $\Re(\mu)$ ($\Re(\mu) \approx -1$) with reduced $\Im(\mu)$.

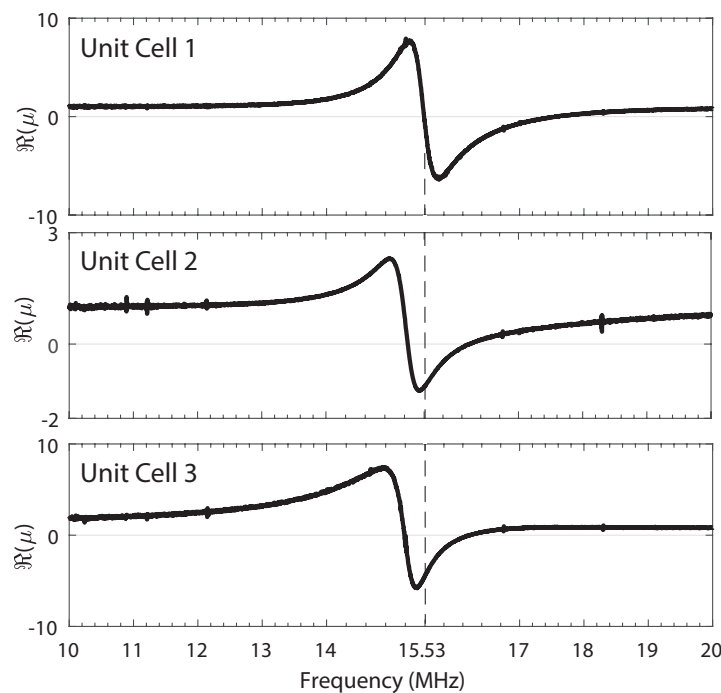


Fig. 2. Measurements results for the real part of the effective magnetic permeability $\Re(\mu)$.

III. TRANSFORMATION OPTICS APPLIED TO FLAT LENS

The way that metamaterial lenses alter the field path inside and outside them is related to their inhomogeneous and anisotropic electromagnetic properties. Therefore, it is possible to design a material in order to get a specific field path. It can be accomplished by using a technique called Transformation Optics (TO) which has been extensively used in order to design novel metamaterial devices [25]. In this technique, the field path manipulation is expressed as a coordinate system transformation. Once Maxwell's equations are invariant to this transformation, the electric permittivity ϵ^* and magnetic permeability μ^* tensors in this new coordinate system is related to the homogeneous properties (ϵ, μ) in Cartesian coordinates through Eq. 4 and Eq. 5, where \mathbb{J} is the Jacobian matrix operator [26].

$$\epsilon^* = \frac{\mathbb{J}\epsilon\mathbb{J}^T}{\det(\mathbb{J})}, \quad (4)$$

$$\mu^* = \frac{\mathbb{J}\mu\mathbb{J}^T}{\det(\mathbb{J})} \quad (5)$$

In this work, TO is used to find the unit cell arrangements which lead to convergent and divergent lenses. This technique reveals the refractive index profile in the device required to alter the field path in the desired way. Once each unit cell has a different refractive index, they can be positioned in order to reproduce this profile [27]. Therefore, a coordinate system transformation is proposed to represent converging and diverging lens by hyperbolically stretching the Cartesian system only in \hat{y} direction. This new system (x', y') in the xy -plane can be expressed as a function of the Cartesian coordinates (x, y) through Eq. 6:

$$\begin{cases} x' = x \\ y' = d_f \pm \alpha \left| \frac{x}{x^2 - a^2} \right| y \end{cases}, \quad (6)$$

where a is the lens radius, d_f is the focal point, α is a scaling factor, the negative signal is used for converging and positive for diverging lens. These new (x', y') coordinate systems are represented in Fig. 3(a) and (b).

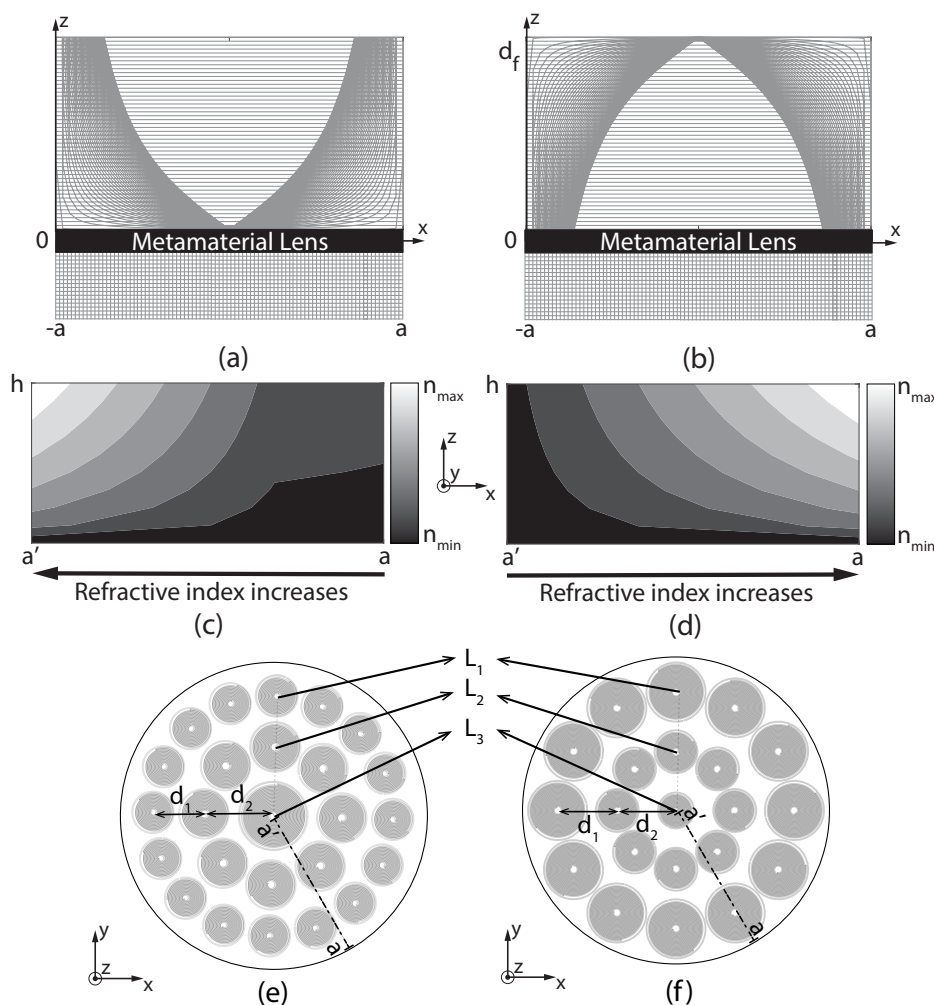


Fig. 3. Conformal transformation that lead to a (a) diverging profile and a (b) converging profile, resulting refractive index profile after application of transformation optics (c-d), and final lens structure with radial periodicity for the (e) diverging and (f) and converging lens.

Considering this coordinate system transformation and by applying the TO procedure, the permittivity and permeability in the transformed coordinate system are given by Eq. 4 and Eq. 5. Therefore, the refractive index can be calculated through $n^* = \sqrt{\mu^* \epsilon^*}$. In Fig. 3(c) and (d) are shown the refractive index profiles calculated in the substrate cross-sections a-a' (h is the substrate thickness) for the diverging and converging lens, respectively. It is important to point out that these refractive index profiles obtained by applying TO represent a hypothetical engineered material, inhomogeneous and anisotropic, which would lead to the desired field distribution. In the practical application of this approach, the substrate is still FR4 which is ideally homogeneous and isotropic. In this case, the geometrical structure of the unit cells and their periodic distribution leads to an effective refractive index distribution that mimics the one provided by TO.

Based on the refractive index profiles in Fig. 3(c) and Fig. 3(d), it can be stated that, in order to design a converging metamaterial lens, the unit cells must be positioned in a way that those with higher refractive index are in the border and it decreases towards the center. On the other hand, the unit cell refractive index must decrease towards the border for a diverging lens. This behavior can be explained by the fact that, from Fermat's principle, the wave path between two points is related to the integral of the refractive index over the line between these two points [28]. Therefore, creating a gradient in the effective refractive index along the metasurface changes the wave path to reproduce the desired field collimation.

From simulations, it was observed that the larger the unit cell, higher the refractive index, as revealed in Table I. Therefore, starting from the center, the unit cell order must be 1, 2, 3 for converging and 3, 2, 1 for diverging lens. In order to alter the field path, as shown in Fig. 3 (a) and (b) in all directions, the stated unit cell orders are revolved along the azimuthal plane which lead to the metamaterial full-structures presented in Fig. 3(e) for the diverging lens, and 3(f) for the converging lens.

Finally, the validity and applicability of the qualitative approach for transformation optics proposed in this work must be discussed. The most common way to apply TO for designing optical devices is to reproduce physically the complex permittivities and permeabilities found in the application of this method to achieve the desired electromagnetic behavior. It can be done by creating chemically and topologically this electromagnetic profile in engineered structures. Even though this is a complex process, it is still feasible for high frequencies, in which the wavelength is very short such as in optics and photonics [29]. However, for applications in lower microwave frequencies, modulating the material properties is much more challenging once even subwavelength unit cells present considerable dimensions. Therefore, a more significant number of unit cells would be required, and the lenses would be prohibitively large. On the other side, the qualitative approach to TO in which the calculated electromagnetic profiles are used as a guideline for positioning the unit cells can also be applied to control the electromagnetic wave propagation. Although a precise control such as accurately defining a focal point is not possible, it still allows focusing around the desired direction, as is the case for designing the converging and diverging lenses. Moreover, in the case of tunable unit cells whose properties can be electronically adjusted, it is possible to achieve collimation control in other directions.

IV. METAMATERIAL LENS DESIGN AND TESTING

The full converging and diverging metamaterial lenses are proposed based on their respective refractive index profiles obtained with TO and the designed unit cells radially positioned with the spacings

d_1 and d_2 between unit cells layers. These spacings were optimized to get $\Re(\mu) < 0$ with a compact structure, and this problem is formulated in Eq. 7:

$$\begin{aligned} & \underset{\hat{\mathbf{x}}}{\text{maximize}} && -\Re[\mu(\hat{\mathbf{x}})] \\ & \text{where} && \hat{\mathbf{x}} = [f, d_1, d_2] \\ & \text{subject to} && d_1 + d_2 + \frac{d_{UC1}}{2} \leq 150 \text{ mm for the diverging lens} \\ & && d_1 + d_2 + \frac{d_{UC3}}{2} \leq 150 \text{ mm for the converging lens,} \end{aligned} \quad (7)$$

where d_{UC1} and d_{UC3} are respectively the diameters of unit cell 1 and 3. However, the inductive and capacitive couplings between unit cells change the total inductance and capacitance, thus shifting the resonant frequency of the full structures to 17.994 MHz . Therefore after optimizing the first lens and verifying this frequency deviation, the spacings of the second lens were optimized according to Eq. 7 but also imposing that its resonant frequency must be 17.994 MHz . Consequently, both lenses can be tested at the same resonant frequency. Apart from that, the optimization procedure and settings follow the same description for optimizing the unit cells presented in section II. The optimization processes resulted in $d_1 = 46.71 \text{ mm}$ and $d_2 = 63.29 \text{ mm}$ for the diverging lens, and $d_1 = 63 \text{ mm}$ and $d_2 = 62 \text{ mm}$ for the converging lens. After that, the lenses were built by assembling each unit cell, etched on an FR4 board, into the full structure in Fig. 3(e-f) and considering the optimized spacings.

The experiment setup to test the metamaterials lenses is shown in Fig. 4. A transmitter coil with the same area as the metamaterial slab is powered by a signal generator, which applies a sinusoid continuous waveform (CW) signal at the metamaterial operation frequency ($f = 17.994 \text{ MHz}$) and magnitude of 23 dBm . A circular loop probe with radius $R = 19.5 \text{ mm}$ is connected to the spectrum analyzer Fieldfox N9912A, and the induced voltage (V_{ind}) is measured at the positions L_1, L_2 , and L_3 indicated in Fig. 3(e-f) as a function of the distance d_{lens} [30]. As the loop probe is much smaller than the transmitter coil, the magnetic field inside the probe can be assumed homogeneous, and the magnetic flux density magnitude ($|\mathbf{B}|$) can be calculated using Eq. 8:

$$|\mathbf{B}| = \frac{V_{ind}}{2f\pi^2R^2}. \quad (8)$$

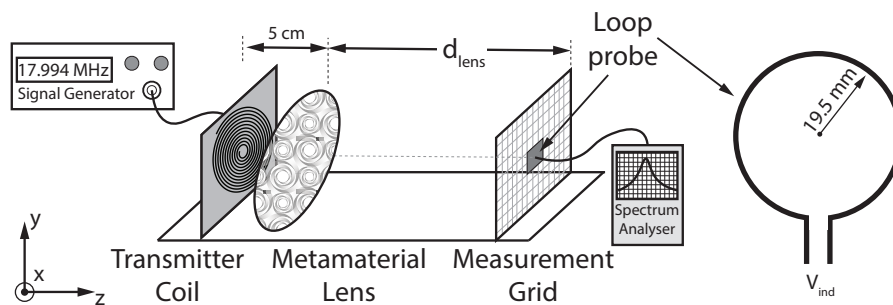


Fig. 4. Metamaterial lens testing and magnetic field measurement setup.

The magnetic flux density magnitudes calculated from the induced voltage measurements are shown in Fig. 5. In the measurements without any lens, it is possible to see that the variation on the field magnitude between the three measurement positions is much less intense than after the inclusion of the metasurfaces. Even though the field intensity, in this case, is higher at the center, it is due to the field

distribution produced by the transmitting coil. After inserting the diverging lens, the field magnitude increases at the border (L_1), decreasing towards the center (L_3). At the center, the behavior with and without lens is practically equal. Conversely, when the converging lens is used, its effects at the border are closer to the measurements without the lens. However, as the loop probe goes to the center, the magnetic field magnitude sharply increases, as was expected for the converging lens. It is important to notice that, at the intermediate position (L_2), the diverging and converging lenses have shown a similar effect on the field amplitude.

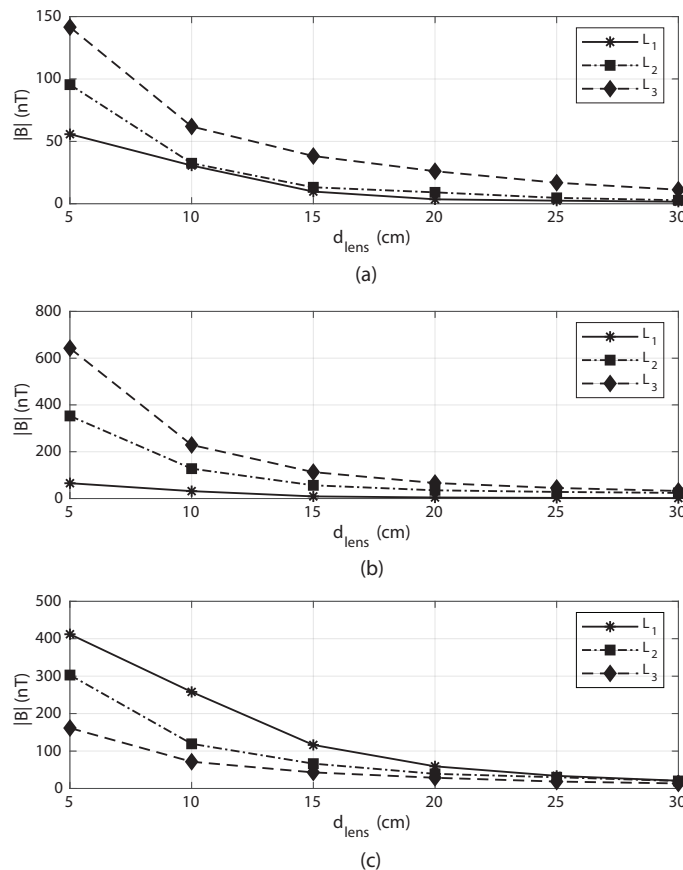


Fig. 5. Measured magnetic flux density at the position L_1 (border), L_2 (intermediate position) and L_3 (center) for the setups (a) without lenses, (b) with the converging lens, and (c) with the divergent lens.

V. WIRELESS POWER TRANSFER EXPERIMENTS

In order to measure the resonant wireless power transfer efficiency, with and without the metamaterial lens, the same experiment setup used to test the magnetic field collimation shown in Fig. 4 was applied. However, the measurement grid and the loop probe were replaced by a receiver coil identical to the transmitter one.

First, to measure the RWPT efficiency (η) as a function of the frequency, the transmitter coil was connected to Port 1 in the vector network analyzer, the receiver coil to Port 2, and the distance between them d_{Tx-Rx} was set to 20 cm. In this way, from the forward complex transmission coefficient (S_{21}) measurements, the RWPT efficiency can be calculated using Eq. 9 [13]:

$$\eta = |S_{21}|^2. \quad (9)$$

This procedure was performed first without the lens. Then, the diverging lens was inserted between the transmitter and receiver coils. The same procedure was repeated for the converging lens. The results of these test are presented in Fig. 6(a).

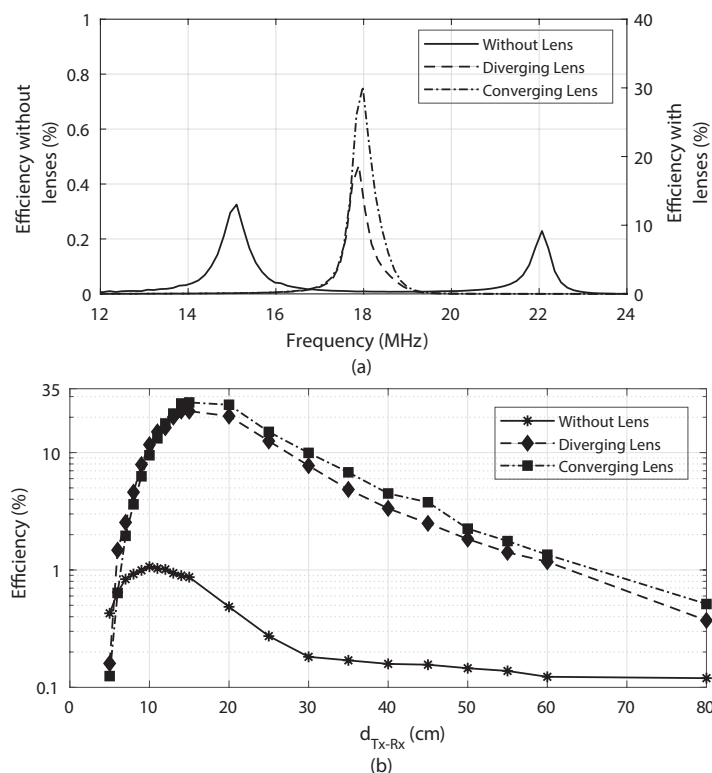


Fig. 6. Wireless power transfer efficiency as a function of (a) frequency and (b) distance between transmitter and receiver.

Without lenses, the power transfer efficiency levels are lower when compared with the results after the lens inclusion. This is due to the fact that the transmitter and receiver coil are loosely coupled, and the frequency splitting phenomenon degrade the RWPT performance. As it can be seen, the maximum efficiency is shifted to 15.11 MHz (0.32%) and 22.06 MHz (0.23%), instead of 17.994 MHz. However, with the metamaterials lens, the efficiency is significantly increased. For the diverging lens, the maximum efficiency was 18.69% and, for the converging lens, 30.16%. In addition, frequency splitting was not verified for both lenses in the analysed frequency and distance ranges.

In most of the previous works [14]–[19], the metamaterial lenses are positioned at the middle between the transmitter and the receiver; however, it reduces the effective range once there is a structure between them. For this reason, in this work, the distance between the transmitter coil and the metamaterial lens was set to 5 cm. Finally, a signal generator was connected to the transmitter coil, and a sinusoidal signal of 23 dBm was applied, at the frequency of maximum efficiency in the previous test (15.11 MHz without the lens and 17.994 MHz with lens). Then, the received power was measured while varying the receiver coil position. These measurements were carried out without the lens and, after that, with the diverging and converging lenses. From these measurements, the RWPT efficiency was calculated as the ratio between received and transmitted power.

The results of these tests are presented in Fig. 6(b) and they are in agreement with the previous experiment. Without the lenses, the maximum power transfer efficiency (1.07%) is achieved when the distance between the transmitter and receiver coil is about 10 cm. On the other side, when the

metamaterial lenses are inserted this efficiency increases as well as the transmission range.

On both experiments, it can be noticed that the efficiency with the diverging lens is slightly lower than with the converging one. This is due to the fact that in these experiments, the transmitter and the receiver coil have the same size and they are aligned. This setup was chosen once in this way, all the tested cases were under the same conditions. However, as shown in this work, the magnetic field is collimated in different positions. The alignment between coils favors the performance with the converging lens, once the magnetic field is focused at the center of the receiver coil. On the contrary, when the diverging lens is used, the field magnitude is higher at the receiver extremity; therefore, the induced voltage, in this case, is lower.

VI. CONCLUSION

In this paper, two kinds of metamaterial lenses have been proposed to improve resonant wireless power transfer systems. Firstly, three unit cells were optimized and simulated using the software CST® in order to get negative magnetic permeability in the same frequency with a different refractive index. It was observed through simulation that larger the unit cell, higher is the refractive index. The prototypes of these three unit cells were built and their permeability calculated from S-parameter measurements.

Then, TO was applied to find the ideal unit cell disposition. In this technique, two transformed coordinate systems were proposed to represent the magnetic field manipulation by a converging and a diverging lens. From the Jacobian matrix operator, the permittivity and permeability tensors can be calculated in the new coordinate system; thus, it is possible to calculate the refractive index in each lens. It has been shown that, in order to produce a converging lens, the unit cell must be positioned in such a manner that the refractive index gradient points toward the lens border, while for the diverging one, this gradient must point toward its center.

Applying the results of TO analysis, a converging and a diverging lens were designed using CST® by optimizing the separation between unit cells. Due to inductive and capacitive couplings between them, it was observed a frequency shift. However, both metamaterial lenses still operating at the specified frequency range. Afterwards, the voltage induced in a probe coil by the sinusoidal magnetic field from a transmitter coil was measured as a function of the distance from the lens for three positions: at the center, in the middle and in the lens border. From these measurements, it was possible to calculate the magnetic flux density magnitude in each position. As expected, the converging lens focuses the magnetic field along the lens center while for the diverging lens, the field magnitude is more intense at the border.

Finally, the designed lens performance in a resonant wireless power transfer system was evaluated as a function of the frequency and the distance between transmitter and receiver coils. It is shown that the metamaterials lenses increase the coupling between these coils, and they reduce the effects of frequency splitting when compared with the same system without lenses, significantly improving the power transfer efficiency and range.

Even though previous works have demonstrated the benefits of metamaterials lens in power transfer applications, the convergent and divergent lenses proposed in this work reveal that the magnetic field can be manipulated in order to focus it in a convenient manner so that the transmitter and receiver coil can be in different sizes and alignments. Furthermore, the lenses used in this paper are positioned in front of the transmitter coil, and they do not need to be placed in the middle of the wireless power transfer system. The presented behavior can lead to coil size reduction, range and efficiency improvement.

ACKNOWLEDGMENTS

This work was partially supported by FAPEMIG, CAPES, CNPq and CEFET-MG.

REFERENCES

- [1] N. Tesla, "Apparatus for transmitting electrical energy," U.S. Patent 1,119,732, Dec. 1, 1914.
- [2] P. Pinho, *Recent wireless power transfer technologies*, 1st ed. IntechOpen, 2020.
- [3] D. Brizi, J. P. Stang, A. Monorchio, and G. Lazzi, "A compact magnetically dispersive surface for low-frequency wireless power transfer applications," *IEEE Transactions on Antennas and Propagation*, vol. 68, no. 3, pp. 1887–1895, 2020.
- [4] T. J. Cui, R. Liu, and D. Smith, *Metamaterials: Theory, Design, and Applications*, 1st ed. Springer-Verlag US, 2010.
- [5] V. G. Veselago, "The electrodynamics of substances with simultaneously negative values of ϵ and μ ," *Soviet Physics Uspekhi*, vol. 10, no. 4, pp. 509–514, apr 1968.
- [6] J. B. Pendry, A. J. Holden, W. J. Stewart, and I. Youngs, "Extremely low frequency plasmons in metallic mesostructures," *Phys. Rev. Lett.*, vol. 76, pp. 4773–4776, Jun 1996.
- [7] J. B. Pendry, A. J. Holden, D. J. Robbins, and W. J. Stewart, "Magnetism from conductors and enhanced nonlinear phenomena," *IEEE Transactions on Microwave Theory and Techniques*, vol. 47, no. 11, pp. 2075–2084, 1999.
- [8] Y. Xuan and X. Xu, "Three-dimensional reciprocal invisibility cloak with multilayered structure," *Journal of Microwaves, Optoelectronics and Electromagnetic Applications*, vol. 18, no. 2, p. 184–195, Apr. 2020.
- [9] A. C. R. de Brito, A. S. de Abreu, A. G. D' Assunção, and C. Peixeiro, "Effects of an fss reflector on a microstrip line fed bow-tie slot antenna," *Journal of Microwaves, Optoelectronics and Electromagnetic Applications*, vol. 19, no. 3, p. 309–326, Jul. 2020.
- [10] C. W. Broadman, C. J. Naify, M. J. Lee, and M. R. Haberman, "Design of a one-dimensional underwater acoustic leaky wave antenna using an elastic metamaterial waveguide," *Journal of Applied Physics*, vol. 129, no. 19, p. 194902, 2021.
- [11] C. Hu, J. Weng, Y. Ding, B. Liang, J. Yang, and J. Cheng, "Experimental demonstration of a three-dimensional acoustic hyperlens for super-resolution imaging," *Applied Physics Letters*, vol. 118, no. 20, p. 203504, 2021.
- [12] J. B. Pendry, "Negative refraction makes a perfect lens," *Physical Review Letters*, vol. 85, pp. 3966–3969, Oct 2000.
- [13] B. Wang, K. H. Teo, T. Nishino, W. Yerazunis, J. Barnwell, and J. Zhang, "Experiments on wireless power transfer with metamaterials," *Applied Physics Letters*, vol. 98, no. 25, p. 254101, 2011.
- [14] Y. Urzhumov and D. R. Smith, "Metamaterial-enhanced coupling between magnetic dipoles for efficient wireless power transfer," *Physical Review B*, vol. 83, p. 205114, May 2011.
- [15] J. V. d. Almeida, E. C. d. Silva, M. M. Mosso, and C. A. F. Sartori, "A parametric study of inductive swipt systems assisted by metamaterial using virtual magnetic tl-based channel modeling," *Journal of Microwaves, Optoelectronics and Electromagnetic Applications*, vol. 20, no. 1, pp. 195–207, 2021.
- [16] C. Rong, C. Lu, Y. Zeng, X. Tao, X. Liu, R. Liu, X. He, and M. Liu, "A critical review of metamaterial in wireless power transfer system," *IET Power Electronics*, p. 1–19, 2021.
- [17] D. Huang, Y. Urzhumov, D. R. Smith, K. Hoo Teo, and J. Zhang, "Magnetic superlens-enhanced inductive coupling for wireless power transfer," *Journal of Applied Physics*, vol. 111, no. 6, p. 064902, 2012.
- [18] C. Rong, X. Tao, C. Lu, Z. Hu, X. Huang, Y. Zeng, and M. Liu, "Analysis and optimized design of metamaterials for mid-range wireless power transfer using a class-e rf power amplifier," *Applied Sciences*, vol. 9, no. 1, p. 26, 2018.
- [19] C. Lu, X. Huang, C. Rong, Z. Hu, J. Chen, X. Tao, S. Wang, B. Wei, and M. Liu, "Shielding the magnetic field of wireless power transfer system using zero-permeability metamaterial," *The Journal of Engineering*, vol. 2019, no. 16, pp. 1812–1815, 2019.
- [20] J. Wang, M. P. Leach, E. G. Lim, Z. Wang, Z. Jiang, R. Pei, and Y. Huang, "A conformal split-ring loop as a self-resonator for wireless power transfer," *IEEE Access*, vol. 8, pp. 911–919, 2020.
- [21] M. Bakir, M. Karaaslan, F. Dincer, and C. Sabah, "Metamaterial characterization by applying different boundary conditions on triangular split ring resonator type metamaterials," *International Journal of Numerical Modelling: Electronic Networks, Devices and Fields*, vol. 30, no. 5, p. e2188, 2017.
- [22] O. Turkmen, E. Ekmekci, and G. Turhan-Sayan, "Effects of using different boundary conditions and computational domain dimensions on modeling and simulations of periodic metamaterial arrays in microwave frequencies," *International Journal of RF and Microwave Computer-Aided Engineering*, vol. 23, no. 4, pp. 459–465, 2013.
- [23] Q. Wu, Y. H. Li, N. Gao, F. Yang, Y. Q. Chen, K. Fang, Y. W. Zhang, and H. Chen, "Wireless power transfer based on magnetic metamaterials consisting of assembled ultra-subwavelength meta-atoms," *Europhysics Letters*, vol. 109, no. 6, p. 68005, mar 2015.

- [24] J. V. de Almeida and R. S. Feitoza, "Metamaterial-enhanced magnetic coupling: An inductive wireless power transmission system assisted by metamaterial-based μ -negative lenses," *IEEE Microwave Magazine*, vol. 19, no. 4, pp. 95–100, 2018.
- [25] L. Xu and H. Chen, "Conformal transformation optics," *Nature Photonics*, vol. 9, no. 1, pp. 15–23, 2014.
- [26] A. Abdolali, H. Barati Sedeh, and M. H. Fakhri, "Geometry free materials enabled by transformation optics for enhancing the intensity of electromagnetic waves in an arbitrary domain," *Journal of Applied Physics*, vol. 127, no. 5, p. 054902, 2020.
- [27] H. Eskandari and Tyc, "Controlling refractive index of transformation-optics devices via optical path rescaling," *Scientific Reports*, vol. 9, no. 1, 2019.
- [28] C. Gomez-Reino, M. V. Perez, and C. Bao, *Gradient index optics*, 1st ed. Springer, 2002.
- [29] M. McCall *et al.*, "Roadmap on transformation optics," *Journal of Optics*, vol. 20, no. 6, p. 063001, 2018.
- [30] M. J. Freire and R. Marques, "Near-field imaging in the megahertz range by strongly coupled magnetoinductive surfaces: Experiment and ab initio analysis," *Journal of Applied Physics*, vol. 100, no. 6, p. 063105, 2006.